Research Papers

Ragone plots of material-based hydrogen storage systems

Marco Gambini, Federica Guarnaccia, Michele Manno [*], Michela Vellini

University of Rome Tor Vergata, Via del Politecnico, 1, Rome, 00133, Italy

ARTICLE INFO

ABSTRACT

This paper presents an analytical assessment of the energy–power relationship for different material-based hydrogen storage systems, namely Metal Hydrides (MHs) and Liquid Organic Hydrogen Carriers (LOHCs). Storage systems are subjected to continuous flow discharge processes through suitable control systems to meet constant specific power demands of end users. By means of reasonable assumptions, analytical expressions of the time-dependent degree of hydrogenation (representing the state of charge) are obtained to find the amount of hydrogen discharged (delivered energy) as a function of flow rate (required power). The results are first presented in the form of dimensionless Ragone plots to highlight the dependence of the amount of discharged hydrogen on the required mass flow rate. Numerical examples are presented for a couple of illustrative systems. Moreover, these analytical expressions are shown to produce very similar results to those obtained with the solution of a dynamic model, including, beyond the kinetic equation, mass and energy conservation applied to the reactor. The results show a significant impact of power demand on the released hydrogen for most systems, similar to that of capacitors, due to the dependence of the rate of reaction on the degree of hydrogenation: as a consequence, the amount of energy that can be delivered to an end user decreases substantially with an increase in the required power, resulting in a poor utilisation factor. Based on these results, MHs exhibit almost first-order kinetics and can sustain efficient discharge with theoretical specific power up to 2 kW/kg (rate of chemical energy delivered per unit mass of active substance), corresponding to a discharge duration of the order of 0.25 h; some LOHCs are limited by second-order kinetics and the specific power should be lower than 1 kW/kg, with discharge durations that must be above 2 hour, to ensure effective utilisation of stored hydrogen.

1. Introduction

Hydrogen is widely believed to play a strategic role in future energy systems [1] based on Renewable Energy Sources (RES), as it allows the storage of intermittent non-programmable electricity generated by RES such as wind and solar [2], avoiding unnecessary curtailments [3] and making it possible to meet the needs of different energy sectors by means of green electricity [4] through the principle of sector coupling [5], even in the case of otherwise hard-to-abate sectors [6].

To fulfil its role as an energy carrier in support of RES, an efficient hydrogen storage and transport infrastructure is required to distribute it from generation to use sites [7]. Given the underwhelming characteristics of hydrogen in terms of energy density, several different storage technologies have been proposed and developed over the years, relying on physical processes to increase hydrogen's density (physical hydrogen storage: compressed, cryo-compressed or liquefied hydrogen) or on the property of selected materials to adsorb, absorb, or chemically react with hydrogen (material-based storage) [8]. Among material-based

technologies, Metal Hydrides (MHs) and Liquid Organic Hydrogen Carriers (LOHCs) have interesting properties that can make them suitable for selected applications, even in the case of large-scale storage [9]. MHs have long been proposed as a viable hydrogen storage technology, and the performance of low-temperature MHs, such as $LaNi_5$ and other similar AB_5 alloys, is interesting in terms of energy density and favourable operating conditions [10,11], despite their poor gravimetric density. More recently, LOHCs have attracted the attention of research groups as a promising storage and transport technology [12]: LOHCs have been shown to provide the cheapest option for long-distance, large-volume hydrogen transport [13] and the lowest levelised cost of hydrogen for intercontinental transport if the whole supply chain is considered [14].

An effective hydrogen storage technology must allow the discharged flow rate to be controlled and matched to the end-user demand, which depends on the specific application considered: this is a particular concern in the case of material-based hydrogen storage, as hydrogen

discharge involves desorption from the MH or a dehydrogenation reaction to release hydrogen from LOHCs, and the kinetic characteristics of these reactions must be considered in the design of control systems and may limit the dynamic performance of these storage systems. In general, control systems must act on the reactor pressure or temperature; both desorption and dehydrogenation are endothermic reactions that require a Heat transfer Fluid (HTF) to transfer heat to the reactor [15, 16] . PID or multi-parametric controllers have been adopted to control the output of MH systems [17], with different configurations, taking the HTF flow rate, the HTF inlet temperature, or the discharge valve opening as control variables acting on reactor temperature or pressure; however, the most straightforward way to control hydrogen flow is through the discharge valve opening [18,19]. Similar configurations have recently been considered to control the flow rate in LOHC-based systems. For example, the operation of DiBenzylToluene (DBT) reactors has been controlled by means of PI/PID controllers acting on the burner providing the required heat of reaction [20], or on the HTF temperature and flow rate [21]. Pressure is also a variable that affects the dehydrogenation reaction of LOHCs, as demonstrated for DBT [22] and N-EthylCarbazole (NEC) [23], suggesting the option of controlling the discharged flow rate also through a discharge valve [24], as in the case of MHs.

Hydrogen storage systems are energy storage devices, with the chemical energy of hydrogen being stored and delivered to the end user. As such, specific energy and specific power, that is, the energy and power that can be effectively released per unit mass, are crucial indicators of performance, as for any energy storage device. Specific energy and specific power are represented in so-called Ragone plots, which were introduced by Ragone [25] in 1968 to describe how the useful energy delivered by electrochemical storage devices decreases as the power required by the end user increases. Christen and Carlen provided a generalised theory of Ragone plots for electrochemical devices [26], and Ragone plots were then extended to thermal energy storage systems [27]. Christen then provided a comprehensive discussion of Ragone plots and efficiency of electrochemical and electro-thermal energy storage devices [28].

Material-based hydrogen storage systems have not yet been characterised in terms of Ragone plots, to describe in a comprehensive and systematic way the inverse relationship between power demand and discharged energy, although this was occasionally recognised in the case of MH systems [29]. Therefore, this paper aims to fill this gap in the literature by providing a framework for assessing the energy–power relation in material-based hydrogen storage systems in the context of constant-power applications, as required by the theory of Ragone plots. It is assumed that the power output (i.e. the flow rate discharged) is controlled through a discharge valve that sets the reactor pressure at the value required by the system dynamics; control through HTF properties (inlet temperature or flow rate) is not included in this analysis, to make it possible to obtain analytical expressions describing the Ragone plot under some simplifying assumptions. These plots are a valuable tool to assess the possible fields of application of a storage technology, and therefore, the results and procedure presented in this paper can be useful in comparing different material-based hydrogen storage systems to find the range of energy-to-power ratios that allows an efficient utilisation of each system.

The paper is structured as follows. Section 2 describes the conceptual layout of the system, the equations that model the hydrogen storage behaviour in the case of chemical storage, with particular reference to LOHCs and MHs; the indicators used to assess system performance are described. Section 3 first describes the analytical results that can be obtained from just the equation representing the kinetic behaviour of the systems; then the numerical results obtained with the model including the kinetics, mass, and energy conservation equations are presented, proving that the simplified model produces accurate results. Finally, Section 4 draws conclusions from the results presented in the previous sections.
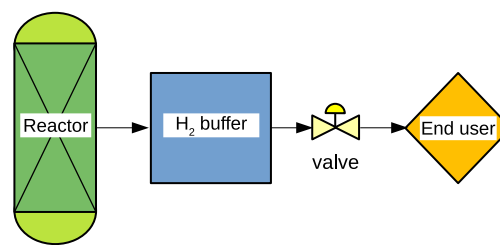

Fig. 1. Conceptual model of the hydrogen storage systems.

2. Methods

This section presents the equations describing the reaction rate and the energy balance of the dehydrogenation reactions, in the case of chemical reactions that are of interest for the chemical storage of hydrogen in substances such as LOHCs or ammonia, or desorption reactions that characterise the operation of MHs.

The reaction rate can be expressed in a dimensionless way through the Degree of Hydrogenation (DoH), that is the ratio of the current hydrogen content $m_{H_2}(t)$ to the maximum hydrogen content possible for a given storage technology, which depends on its gravimetric density w and the mass of the active substance m. If the DoH is indicated for simplicity as x:

$$x(t) = m_{H_2}(t)/m_{H_2,\max} = m_{H_2}(t)/(wm). \tag{1}$$

The choice of a dimensionless variable is useful for comparing different storage technologies. However, in the literature, the kinetic equation is often described with different, non-dimensionless variables, so care must be taken when comparing the numerical values of the parameters used in these equations.

The dehydrogenation rate $\dot{x}$, which corresponds to the reaction rate and is thus a negative quantity as the hydrogen content decreases, is related to the mass flow rate of hydrogen released by the reactor $\dot{m}_{H_2,r}$ through the following equation:

$$\dot{m}_{H_2,r} = -wm\dot{x}. \tag{2}$$

The hydrogen storage system model includes a reactor, which contains the active substance (MH or LOHC) and the heat exchanger required to transfer heat from the HTF, connected to a control valve through a hydrogen-filled volume (Fig. 1), representing the volume available for gaseous hydrogen within the reactor and the connection to the control valve. The valve is controlled to supply a constant mass flow rate $\dot{m}_{H_2,d}$ to the end user (the subscript $_d$ stands for *discharged* by the system to the end user), acting on the pressure inside the reactor. The corresponding constant rate of dehydrogenation is defined as:

$$\dot{x}_d = -\dot{m}_{H_2,d}/(wm) \tag{3}$$

and coincides with the rate of dehydrogenation reached at steady-state conditions (no accumulation of hydrogen inside the buffer).

The ratio of available hydrogen mass and constant mass flow rate discharged to the end user represents the theoretical discharge duration $\tau_{\max}$, that is, the time that would be required to fully discharge the hydrogen storage system for a given value of discharged flow rate:

$$\tau_{\max} = m_{H_2,\max}/\dot{m}_{H_2,d} = (wm)/\dot{m}_{H_2,d} = -1/\dot{x}_d. \tag{4}$$

The actual discharge duration τ is lower than $\tau_{\max}$ because in general energy storage systems supply a decreasing share of stored energy for increasing values of constant power output. This is confirmed for hydrogen storage systems by the results presented in the following.

2.1. Kinetics

2.1.1. Chemical storage

If hydrogen must be released through a chemical dehydrogenation reaction, as in the case of LOHCs and ammonia, the reaction rate can be expressed for a reaction of order n as follows [30]:

$$\dot{x} = -kx(t)^n. \tag{5}$$

In general, the rate constant k depends on the catalyst used, the temperature, and the pressure [23]:

$$\dot{x} = -k_0 \exp\{-E_a/(RT)\} \exp(-bp)\, x(t)^n. \tag{6}$$

Here, k_0 is the frequency factor (or pre-exponential factor) that depends on the particular reaction considered and on the catalyst used; E_a is the activation energy that determines how temperature impacts the reaction through the Arrhenius law; b is a pressure coefficient that takes into account the effect of pressure on kinetics, which is relevant when the number of moles of gaseous substances change as the reaction proceeds, as is usually the case in dehydrogenation reactions.

2.1.2. Metal hydride storage

In the case of metal hydrides, how to model desorption kinetics is still an open issue debated by scholars [31]. Several classical models for reactions in the solid state have been considered, such as contracting area, contracting volume, Prout–Tompkins, Johnson–Mehl–Avrami (JMA) [30,32], and variations on these [31]. In general, the reaction rate can be expressed as the product of an Arrhenius rate constant, a limiting factor depending on operating pressure and equilibrium pressure (which is discussed at the end of this section), and a factor depending on degree of hydrogenation and reaction order [33]:

$$\dot{x} = k(T) f_p(p, p_{eq}) f_x(x). \tag{7}$$

It should be noted that the factor f_p is not entirely independent of the degree of hydrogenation, since the equilibrium pressure depends on it, as shown by Eq. (10); this factor in most cases introduces either a linear [34,35] or a logarithmic [29,36] dependence on pressure [33]. In the case of JMA models, the degree of hydrogenation changes with time according to $x(t) = \exp(-kt^n)$, where the index of reaction n generally can have the values 1.5, 2 and 3; thus, the reaction rate is given by:

$$\dot{x} = k n\, t^{n-1} x(t). \tag{8}$$

However, in many practical cases the simple kinetic model obtained with an index of reaction $n = 1$ has been found to provide reasonably accurate results, validated against experimental results [29,34,35]. Thus, in this paper the reaction rate of MHs has been evaluated as follows [36]:

$$\dot{x} = -k_0 \exp\{-E_a/(RT)\} \log\left(p_{eq}/p\right) x(t). \tag{9}$$

Therefore, the equation is very similar to that describing first-order chemical reaction kinetics, Eq. (6), as it includes the same dependence on a pre-exponential factor k_0 and on the Arrhenius' law (it is not exactly a first-order equation due to the slight dependence of the equilibrium pressure on concentration, described in the following): the difference lies in the logarithmic dependence on pressure, rather than exponential. Moreover, in the case of MHs, the pressure coefficient is replaced by a parameter with precise physical meaning: the equilibrium pressure of MH p_{eq}. In particular, the pressure driver for hydrogen desorption is related to the ratio of the equilibrium pressure to the system pressure: the lower the latter is compared to the equilibrium pressure, the higher the desorption rate, thus representing a thermodynamic driving force for the reaction.

The Van't Hoff law gives the equilibrium pressure as a function of the variation in enthalpy ΔH and entropy ΔS due to the phase change from the dehydrogenated substance (α-phase) to the hydride one (β-phase) [37], corrected to take into account both a slight increase in pressure as hydrogen concentration in the hydride increases, resulting in a slight slope (ϕ_{sl}) of the PCT (pressure-concentration-temperature) curve, and the hysteresis between hydrogen charge and discharge operation quantified by the parameter ϕ_{hys}:

$$\log\left(p_{eq}/p_{ref}\right) = \Delta H/(RT) - \Delta S/R + \phi_{sl}\left(x - x_{ref}\right) + \phi_{hys} \tag{10}$$

where p_{ref} is a reference pressure (usually 1 bar) and x_{ref} is the concentration corresponding to the equilibrium pressure resulting by the uncorrected Van't Hoff law (usually 0.5). In the case of constant-temperature processes, this equation can be written in a shorter form that highlights the linear dependence of equilibrium pressure on hydrogen concentration:

$$\log\left(p_{eq}/p_{ref}\right) = A + \phi_{sl}x \tag{11}$$

where:

$$A = \Delta H/(RT) - \Delta S/R - \phi_{sl}x_{ref} + \phi_{hys}. \tag{12}$$

2.2. Mass conservation equation

The mass conservation equation states that the net flow of hydrogen into the hydrogen volume, which is the difference between the rate of hydrogen released by the reactor $\dot{m}_{H_2,r}$ entering the buffer, Eq. (2), and the constant discharged hydrogen flow rate $\dot{m}_{H_2,d}$ leaving the buffer, must be balanced by the accumulation of hydrogen inside the hydrogen volume V. Neglecting any change in volume of the storage material due to the decreasing degree of hydrogenation, this leads to the following equation:

$$V\frac{d\rho}{dt} = \dot{m}_{H_2,r} - \dot{m}_{H_2,d} = -wm\left(\dot{x} - \dot{x}_d\right) \tag{13}$$

where ρ is the density of gaseous hydrogen in the buffer volume, and Eqs. (2) and (3) have been used to write the rate of change in density in terms of the rate of dehydrogenation.

In the pressure and temperature range that must be considered for material-based hydrogen storage, hydrogen can be safely modelled as an ideal gas, hence the relationship between density, pressure and temperature is:

$$p = \rho RT/M_{H_2} \tag{14}$$

with $M_{H_2} = 2.016\,\text{g/mol}$ being hydrogen's molar mass.

By introducing the quantity:

$$\rho_{max} = V/(wm) \tag{15}$$

and defining the dimensionless density $y_\rho = \rho/\rho_{max}$, the mass conservation equation can be rewritten in the following, dimensionless, way:

$$\dot{y}_\rho = -\left(\dot{x} - \dot{x}_d\right). \tag{16}$$

The quantity ρ_{max} represents the maximum density that could be obtained if the entire amount of hydrogen stored in the system (equal to wm) were released and confined within the available volume V.

2.3. Energy conservation equation

The energy conservation equation states that the change in internal energy of the system is the difference between the rate of heat transferred by the HTF $\dot{Q}_{HTF}$ and the reaction heat rate $\dot{Q}_r$:

$$\frac{dU}{dt} = \dot{Q}_{HTF} - \dot{Q}_r. \tag{17}$$

Neglecting both the change in heat capacity of the system (C) due to the change in degree of hydrogenation and the sensible enthalpy of hydrogen with respect to the reaction enthalpy change, and taking into account the heat transfer effectiveness ε, the energy conservation equation becomes:

$$C\frac{dT}{dt} = \varepsilon \dot{C}_f\left(T_f - T\right) + wm\dot{x}\Delta H \tag{18}$$

where $\dot{C}_f = \dot{m}_f c_f$ is the HTF flow heat capacity and $\dot{Q}_r = wm\dot{x}\Delta H$ is the reaction heat rate determined by the reacting mass flow rate, given by Eq. (2), and the reaction enthalpy ΔH. This equation can be further rearranged to highlight the following parameters: first, the temperature time constant τ_T, defined as:

$$\tau_T = C/\left(\epsilon\dot{C}_f\right). \tag{19}$$

Second, the steady-state reaction heat rate $\dot{Q}_{r,d}$ corresponding to the constant discharged flow rate $\dot{m}_{H_2,d}$:

$$\dot{Q}_{r,d} = -\dot{m}_{H_2,d}\Delta H = -wm\dot{x}_d\Delta H. \tag{20}$$

Finally, the steady-state temperature difference δ:

$$\delta = \dot{Q}_{r,d}/\left(\epsilon\dot{C}_f\right) \tag{21}$$

that represents the temperature difference between HTF and reactor in a constant-temperature discharge process with a constant rate of dehydrogenation $\dot{x} = \dot{x}_d$. With these definitions, the energy conservation equation is replaced by:

$$\tau_T\dot{T} = T_f - T - \delta\dot{x}/\dot{x}_d. \tag{22}$$

For the numerical solution of the equations system it can be useful to replace the reactor temperature T with the variable θ, defined as:

$$\theta = T - \left(T_f - \delta\right). \tag{23}$$

This temperature-related variable is zero in a constant-temperature discharge process with a constant rate of dehydrogenation. The energy conservation equation can thus be written as follows:

$$\tau_T\dot{\theta} = -\theta + \delta\left(1 - \dot{x}/\dot{x}_d\right). \tag{24}$$

2.4. Governing equations

In summary, the hydrogen storage system can be modelled through the following system of three implicit Ordinary Differential Equations (ODEs):

$$\dot{x} = -k_0\exp\{-E_a/(RT)\}f(p)x(t)^n \tag{25}$$

$$\dot{y}_\rho = -\left(\dot{x} - \dot{x}_d\right) \tag{26}$$

$$\tau_T\dot{\theta} = -\theta + \delta\left(1 - \dot{x}/\dot{x}_d\right) \tag{27}$$

where the pressure function appearing in the first equation is either $f(p) = \exp(-bp)$ or $f(p) = \log\left(p_{eq}/p\right)$ for LOHCs and MHs, respectively, and the reaction order n is equal to one for MHs.

2.4.1. Thermodynamic model parameters

Besides the parameters required by the kinetic model, discussed in Section 2.1, the governing equations require three additional parameters: the maximum density ρ_{max}, defined by Eq. (15); the thermal time constant τ_T, Eq. (19); the steady-state temperature difference δ, Eq. (21).

The maximum density was chosen so that the pressure reached inside the buffer if it contained the entire amount of hydrogen stored in the system was 5 MPa at reference temperature (25 °C), resulting in $\rho_{max} = 4.07 \text{ kg/m}^3$ calculated with the assumption of ideal gas.

The thermal time constant was set at $\tau_T = 10$ s in line with previous studies [38]; however, this parameter mostly affects the transient behaviour of the system and is almost irrelevant with respect to the total discharged mass of hydrogen, which is the subject of this study.

The last parameter in the governing equations is the steady-state temperature difference δ. On the basis of its definition, it is directly proportional to the discharged flow rate, so it must be changed accordingly as the required flow rate varies. So, a value of $\delta_{ref} = 15$ K was chosen for the theoretical maximum rate of dehydrogenation, defined later by Eq. (33), and the actual value was then obtained as:

$$\delta = \left(\dot{x}_d/\dot{x}_{max}\right)\delta_{ref}. \tag{28}$$

2.4.2. Initial conditions

In the case of LOHCs, it was assumed that at the start of the process the LOHC is full (for simplicity it is assumed that $x_0 = 1$ even though in practical applications the degree of hydrogenation starts from approximately 95%), and the reactor is in equilibrium with the HTF ($T_0 = T_f \Rightarrow \theta_0 = \delta$) at the minimum pressure ($p_0 = p_{min}$). The choice not to consider a higher pressure level at the start of the process allows the (small) contribution of the buffer to supply hydrogen on top of the chemical reaction to be removed from the results, thus concentrating the analysis on just the reactor.

It was assumed that at the beginning of the process, the reactor is in thermal equilibrium with the HTF in the case of MHs as well; however, the pressure inside the reactor must be the equilibrium pressure resulting from the reactor temperature, given by Eq. (10), leading to a non-negligible mass of hydrogen contained in the buffer available for discharge (since $p_{eq,0} > p_{min}$). To remove as much as possible the influence of the buffer, it was assumed that the mass of hydrogen required to reach the equilibrium pressure inside the buffer is provided by the MH, which, as a consequence, does not start at full hydrogenation ($x_0 < 1$). In particular, the increase in hydrogen density at the start of the process, due to the reactor being at the equilibrium pressure instead of the minimum pressure, is:

$$\Delta\rho = \left(p_{eq,0} - p_{min}\right)M_{H_2}/\left(RT_0\right) \tag{29}$$

The corresponding hydrogen mass is obtained by multiplying by the buffer volume: $\Delta m = V\Delta\rho$. This mass is released by the MH with a decrease in hydrogen concentration given by:

$$\Delta x = \Delta m/(wm) = \Delta\rho/\rho_{max}. \tag{30}$$

Hence, in the case of MHs the initial condition on the degree of hydrogenation is:

$$x_0 = 1 - \Delta x = 1 - \Delta\rho/\rho_{max} = 1 - \left(p_{eq,0} - p_{min}\right)M_{H_2}/\left(RT_0\right). \tag{31}$$

2.5. Performance indicators

The performance of material-based hydrogen storage system was assessed by means of the following quantities:

- dimensionless power;
- dimensionless discharged energy, or utilisation factor;
- specific power;
- specific energy.

The *dimensionless power* Π is the ratio of the discharged flow rate and the maximum possible flow rate, which, according to Eqs. (6) and (9), is obtained for a given temperature and a fully charged storage medium ($x_0 = 1$), with the minimum possible pressure p_{min}:

$$\Pi = \dot{m}_{H_2,d}/\dot{m}_{H_2,max} = \dot{x}_d/\dot{x}_{max} \tag{32}$$

$$\dot{x}_{max} = \dot{x}(x = 1, p = p_{min}). \tag{33}$$

The *dimensionless discharged energy* gives the amount of hydrogen that the system can release in a constant-flow-rate discharge process and is a function of the required flow rate:

$$e(\Pi) = E_d/E_{max} = m_{H_2,d}/m_{H_2,max} = m_{H_2,d}/(wm). \tag{34}$$

The discharge process ends at the time τ when the pressure can no longer be decreased to compensate for the reduction in the degree of hydrogenation, which reaches a final value $x^* = x(\tau) \geq 0$. Therefore, the dimensionless discharged energy is obtained as:

$$e(\Pi) = 1 - x^* \tag{35}$$

which can also be interpreted as the *utilisation factor* for a given power requirement: that is, the mass of hydrogen that can be effectively delivered divided the total mass of hydrogen available in the storage system. Given the constant rate of discharge, the discharged energy E_d

is proportional to the actual duration of discharge τ, while the stored energy $E_{\max}$ is proportional to the theoretical duration of discharge $\tau_{\max}$; hence, the utilisation factor is also given by the ratio of actual to theoretical duration of discharge:

$$e(\Pi) = \tau/\tau_{\max}. \tag{36}$$

The *specific power* $\tilde{P}$ is defined as the rate of chemical energy released per unit mass of active substance:

$$\tilde{P} = \dot{m}_{H_2,d} Q_{HHV}/m = \Pi \, \dot{m}_{H_2,\max} Q_{HHV} = -w \, Q_{HHV} \dot{x}_d \tag{37}$$

where $Q_{HHV} = 141.8\,\text{MJ/kg} = 39.38\,\text{kWh/kg}$ is hydrogen's higher heating value.

Finally, the *specific energy* discharged is the chemical energy that the system can release per unit mass of active substance:

$$\tilde{E}(\tilde{P}) = m_{H_2,d} Q_{HHV}/m = w \, Q_{HHV} e(\Pi). \tag{38}$$

It is useful to verify that the specific energy-to-power ratio in the case of full utilisation of the hydrogen stored in the system ($e = 1$) coincides with the theoretical discharge duration, defined by Eq. (4): $\tilde{E}_{\max}/\tilde{P} = -1/\dot{x}_d = \tau_{\max}$. As a consequence, the theoretical discharge duration, or the discharge duration coupled to the utilisation factor, can be used to identify the power required by the end user once the stored energy has been set:

$$\tilde{P} = \tilde{E}_{\max}/\tau_{\max} = e\tilde{E}_{\max}/\tau. \tag{39}$$

3. Results and discussion

3.1. Simplified model

The model presented in Section 2 includes the effects of reaction kinetics, along with mass and energy conservation in the reactor, resulting in the "full" model described by Eqs. (25)–(27). However, the constant-flow-rate discharge process was first assessed by means of a simplified model, consisting of just the kinetics Eq. (25), which can be obtained from the "full" model with the assumption of constant temperature and a negligible effect of the capacitance of the hydrogen volume (buffer). The simplified model is particularly useful as it makes it possible to find an analytical solution representing the discharge process and, hence, a closed-form equation for the Ragone plots, as shown in this Section.

Thus, the model has been first simplified with the assumption of a constant-temperature discharge and neglecting the capacitance effect of the hydrogen volume. Under these assumptions, there is no accumulation of hydrogen; hence, the rate of hydrogen released by the reactor is instantaneously equal to the discharged flow rate:

$$\dot{m}_{H_2,r} = \dot{m}_{H_2,d} \Rightarrow \dot{x} = \dot{x}_d. \tag{40}$$

The required dehydrogenation rate is obtained by the control system acting on the control valve to adapt the pressure inside the reactor to the change in degree of hydrogenation, taking into account the kinetics represented by Eq. (9) or (6) for MHs or LOHCs, respectively. In particular, the degree of hydrogenation decreases linearly with the hydrogenation rate ($\dot{x} < 0$):

$$x(t) = 1 + \dot{x}t \tag{41}$$

and the reactor pressure must be decreased accordingly, by gradually opening the control valve, to maintain the required flow rate, until it reaches a minimum value $p_{\min}$, which in practice is equal to the back-pressure set by the end-user equipment (under the assumption of negligible pressure drop through the control valve at its maximum opening).

In the case of the simplified model, the governing Eqs. (25)–(27) thus reduce to just the kinetic Eq. (25), which can be solved analytically, as shown in the next paragraphs.

3.1.1. Metal hydrides

In the case of metal hydrides, the kinetic equation, Eq. (9), can be manipulated to highlight the terms depending on pressure (which is used to control the flow rate at a constant value) on the one hand and hydrogen concentration on the other:

$$\dot{x} = k_T \left[K(p) + \phi_{sl} x(t) \right] x(t) \tag{42}$$

where $k_T = k_0 \exp\{E_a/(RT)\}$, and the following function of pressure has been introduced:

$$K(p) = A - \log p/p_{ref} = \Delta H/(RT) - \Delta S/R - \phi_{sl} x_{ref} + \phi_{hys} - \log p/p_{ref}. \tag{43}$$

The assumption of a constant dehydrogenation rate ($\dot{x} = \text{const.}$) leads to a second-order algebraic equation in the unknown $x(t)$:

$$\phi_{sl} x^2 + K(p)x - \dot{x}/k_T = 0 \tag{44}$$

which yields:

$$x(t) = \frac{K(p)}{2\phi_{sl}} \left(\sqrt{1 + \frac{4\phi_{sl}\dot{x}}{k_T K(p)^2}} - 1 \right) \tag{45}$$

By introducing the following dimensionless quantity:

$$a(p) = \phi_{sl}/K(p) \tag{46}$$

the degree of hydrogenation can be expressed as:

$$x(t) = \frac{1}{2a(p)} \left(\sqrt{1 + \frac{4a(p)\dot{x}}{k_T K(p)}} - 1 \right). \tag{47}$$

In the case of a negligible plateau slope ($\phi_{sl} \to 0$), the second-order term vanishes and the solution is:

$$\lim_{\phi_{sl} \to 0} x(t) = \frac{\dot{x}}{k_T K(p)}. \tag{48}$$

The maximum rate of dehydrogenation is obtained, for a given temperature, at the start of the process when the system is fully charged ($x_0 = 1$: in the case of the simplified model the hydrogen release, Eq. (30), required to reach the equilibrium pressure in the buffer is neglected), with the minimum pressure $p_{\min}$ allowed by the control system:

$$\dot{x}_{\max} = k_T \left(K(p_{\min}) + \phi_{sl} \right) = k_T K(p_{\min}) \left(1 + a_{\max} \right) \tag{49}$$

where $a_{\max} = \phi_{sl}/K(p_{\min})$ is the value of $a(p)$ resulting from the minimum pressure. Hence, the dimensionless equivalent power is given by:

$$\Pi = \frac{\dot{x}}{\dot{x}_{\max}} = \frac{\dot{x}}{k_T K(p_{\min}) \left(1 + a_{\max} \right)}. \tag{50}$$

Hydrogen can be discharged by the system as long as $p \geq p_{\min}$, as it is not possible to further increase the pressure driver of dehydrogenation to compensate for the decrease in the degree of hydrogenation; therefore, the final degree of hydrogenation $x^* = x(\tau)$ is obtained by substituting $a(p) = a_{\max}$ and $K(p) = K(p_{\min})$ in Eq. (47):

$$x^* = \frac{1}{2a_{\max}} \left(\sqrt{1 + 4a_{\max} \left(1 + a_{\max} \right) \Pi} - 1 \right) \tag{51}$$

and the dimensionless equivalent discharged hydrogen results from $e = 1 - x^*$:

$$e(\Pi) = 1 - \frac{1}{2a_{\max}} \left(\sqrt{1 + 4a_{\max} \left(1 + a_{\max} \right) \Pi} - 1 \right). \tag{52}$$

If the plateau slope is neglected:

$$\lim_{a^* \to 0} e(\Pi) = 1 - \Pi \tag{53}$$

corresponding to the discharge of a first-order kinetic equation, as demonstrated later. Since plateau slopes are generally low, in most cases $a_{\max} \ll 1$ and the Ragone plot of MHs is very close to that corresponding to first-order kinetics.

Table 1
Material properties of LaNi$_5$, NEC, and DBT.

Parameter	LaNi$_5$	NEC	DBT
Gravimetric density w/% [9,23,40]	1.8	5.8	6.2
Desorption reaction enthalpy change ΔH/(kJ/mol) [40]	−30.1	–	–
Desorption reaction entropy change ΔS/(J/(mol K)) [40]	−109.96	–	–
Plateau slope ϕ_{sl} [36,41]	0.09	–	–
Pre-exponential factor k_0/s^{-1} [23,36,39,41]	9.57	4.35×10^{10}	3.36×10^6
Activation energy E_a/(kJ/mol) [23,36,39,41]	16.42	121.0	119.8
Pressure coefficient b/bar^{-1} [22,23]	–	1.397	0.0922

In the case of LaNi$_5$ the properties related to equilibrium and kinetic performance are summarised in Table 1. The equilibrium pressure at 25 °C is $p_{eq} = 2.95$ bar, and setting $p_{min} = 1$ bar, the quantities that define the dimensionless discharged energy have the following values: $K(p_{min}) = 1.083$; $k_T = 1.86 \times 10^{-3}$ s^{-1}; $a_{max} = 0.0831$.

3.1.2. LOHCs

The kinetic equation that can be taken into consideration for LOHCs, Eq. (6), results in a much simpler expression of dimensionless energy as a function of dimensionless power.

The maximum dehydrogenation rate is again obtained, for a given temperature, at the start of the discharge process ($x_0 = 1$), with the minimum pressure p_{min} allowed by the control system:

$$\dot{x}_{max} = k_T \exp\left(-b p_{min}\right). \tag{54}$$

The degree of hydrogenation is given by the following equation:

$$x(t) = \left[\frac{\dot{x}}{k_T \exp\left(-bp\right)}\right]^{1/n}. \tag{55}$$

The discharge process ends when the minimum pressure is reached, with the following final degree of hydrogenation:

$$x^* = \left[\frac{\dot{x}}{k_T \exp\left(-b p_{min}\right)}\right]^{1/n} = \left(\dot{x}/\dot{x}_{max}\right)^{1/n} = \Pi^{1/n} \tag{56}$$

so that the dimensionless discharged energy, corresponding to the utilisation factor, is:

$$e(\Pi) = 1 - \Pi^{1/n}. \tag{57}$$

The dimensionless Ragone plot for constant-temperature LOHCs thus depends only on the reaction order. For example, both DiBenzylToluene (DBT) and N-EthylCarbazole (NEC) are characterised by second-order kinetics [23,39].

3.1.3. Ragone plots

The dimensionless Ragone plot of MH and LOHC hydrogen storage systems resulting from the simplified model is shown in Fig. 2, for first- and second-order kinetics in the case of LOHCs. Since the dehydrogenation rate depends on the degree of hydrogenation in all three systems, the amount of discharged hydrogen decreases with the required flow rate, and it tends to zero as the flow rate approaches its maximum value, meaning that theoretically the maximum flow rate can only be sustained for an infinitesimally short time.

The corresponding Ragone plots representing the specific energy, resulting from Eq. (38), against specific power, given by Eq. (37), are shown in Fig. 3 for an MH system based on LaNi$_5$ and for LOHC systems based on NEC or DBT. The properties required to evaluate Ragone plots are available in the literature and are listed in Table 1, together with the sources from which they were derived. In the case of DBT, the pressure coefficient b was estimated based on the reactor response to a change in reactor pressure [22].

It is worth recalling that the specific power and energy derived from Eqs. (37) and (38) are calculated per unit mass of the active substance and do not consider the entire mass of the hydrogen storage system: therefore, the practical values of these quantities would be unavoidably lower, and this is why the results presented in Fig. 3 are indicated as
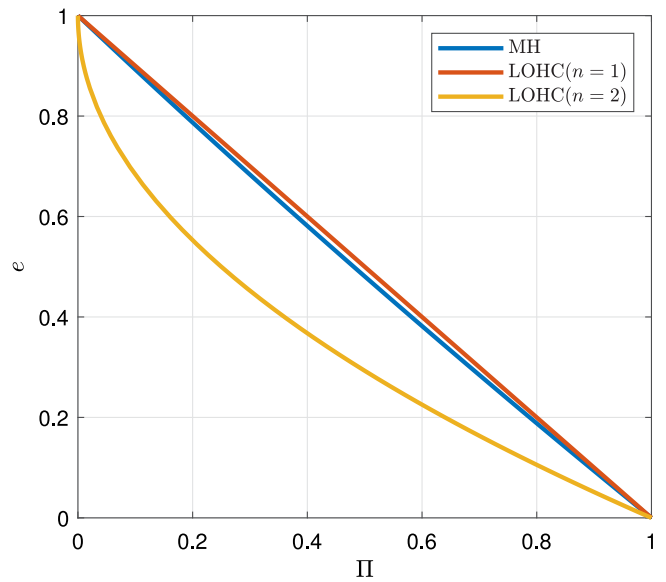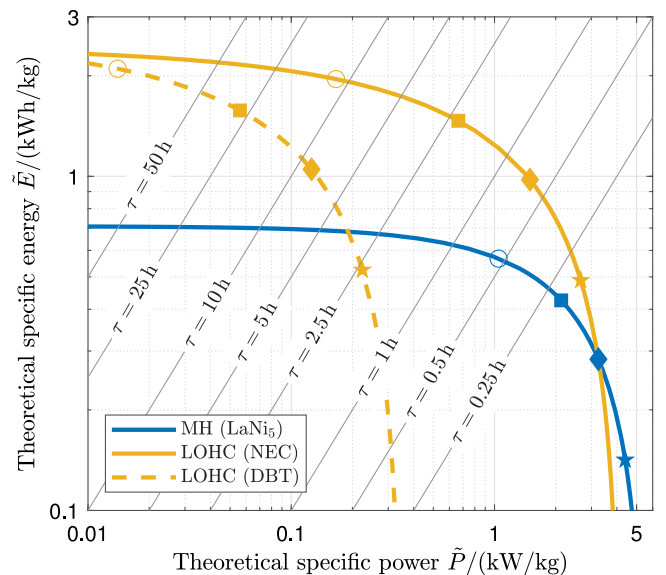

Fig. 2. Dimensionless Ragone plot.

Fig. 3. Representative Ragone plot of hydrogen storage systems based on LaNi$_5$, NEC and DBT. Markers indicate the utilisation factors (○ 80%; ■ 60%; ◆ 40%; ★ 20%).

theoretical. However, the additional mass on top of that of the active substance affects both energy and power in the same way, meaning that the Ragone plot would retain the same shape, only scaled towards lower values.

The Ragone plot in Fig. 3 highlights some notable characteristics of the hydrogen storage systems discussed here. In general, LOHCs

can reach higher specific energy values than MHs due to the higher gravimetric density w; however, the specific power (related to the discharged mass flow rate per unit mass of active substance) has similar ranges for the two storage options, since it is not affected by the gravimetric density but by the kinetic properties of the reaction involved. Clearly, the range of specific flow rates that can be obtained by these storage systems depends on the kinetic properties of the active substance and the reactor, which may differ even significantly due to catalyst used, reactor configuration, etc. However, the order of magnitude is reasonably identified by the Ragone plot.

More importantly, the Ragone plot highlights the range of energy-to-power ratios, represented by the discharge duration τ, which results in acceptable levels of utilisation factors. In other words, the Ragone plot suggests a threshold energy-to-power ratio below which it is impossible to effectively use the hydrogen stored in the system, as a substantial amount cannot be discharged in a constant-flow-rate discharge process (it could be delivered only by reducing the flow rate to the end user). With the parameters used to model LaNi$_5$ properties, represented in Table 1, the Ragone plot (Fig. 3) shows that a hydrogen storage system based on this MH can operate with a utilisation factor above 60% with energy-to-power ratios as low as 0.25 h; instead, LOHC-based systems appear to be more suitable for longer discharge durations, with 25 h and 2.5 h required to achieve the same 60% utilisation factor for DBT and NEC, respectively.

3.2. Full model

In the case of the full dynamic model, the system of governing equations, Eqs. (25)–(27), must be solved numerically, so the resulting implicit ODE system was implemented in Matlab and solved with the `ode15i` function. Figs. 4 and 5 show the resulting evolution over time of a LaNi$_5$- and NEC-based hydrogen storage system, respectively, for representative values of theoretical discharge duration.

The behaviour of the MH-based reactor (Fig. 4) is markedly influenced by the MH equilibrium pressure and the initial conditions of thermal and mechanical equilibrium between MH and gaseous hydrogen. As the valve opens to start the constant-flow rate discharge process, it is the buffer, rather than the desorption reaction, that supplies most of the hydrogen, given the relatively high pressure and the mechanical equilibrium that make the contribution of the pressure driver in Eq. (9) irrelevant. Therefore, at the beginning of the process, the rate of dehydrogenation starts with relatively low values and the degree of hydrogenation does not decrease linearly (starting from an initial value lower than one, as discussed in Section 2.4.2). However, the buffer is soon depleted from excess hydrogen, so the reaction rate must sustain almost the whole flow rate required ($\dot{x} \cong \dot{x}_d$), and the degree of hydrogenation decreases linearly; in the meantime, the pressure must also decrease to a value that is suitably lower than the equilibrium pressure to sustain the reaction. The process can continue until the minimum pressure is reached.

The situation is different in the case of the LOHC-based reactor (Fig. 5), due to the different assumptions regarding the initial conditions and, most importantly, the different nature of the pressure driver on the reaction kinetics that does not involve an equilibrium pressure. Therefore, at the beginning of the process, there is a strong pressure driver ($p_0 = p_{\min}$) and there is a relatively fast dehydrogenation, with reaction rates even higher than those required by the discharged flow rate ($\dot{x}_0 > \dot{x}_d$), which not only supplies hydrogen to the end user, but also fills the buffer, resulting in an increase in pressure that slows down the reaction. After this transient, a dynamic equilibrium condition is reached where the reaction rate meets the needs of the end user without the help of the buffer; however, the pressure inside the buffer cannot remain constant because the decrease in the degree of hydrogenation must be compensated by a decrease in pressure to maintain a constant reaction rate, as required by Eq. (6). The process continues until the time instant τ when the minimum pressure is reached: based on Fig. 5,
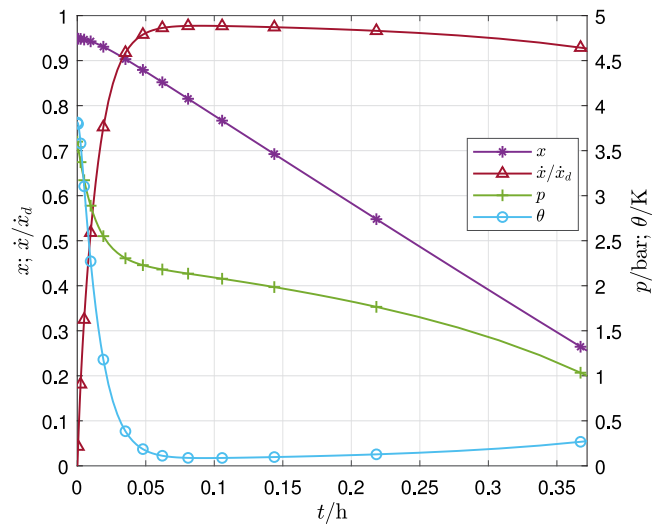

Fig. 4. Constant-flow rate discharge process of a LaNi$_5$-based hydrogen storage system; theoretical discharge duration $\tau_{\max} = 0.5\,\text{h}$ (dimensionless power $\Pi = 25.4\,\%$, utilisation factor 74.4%).
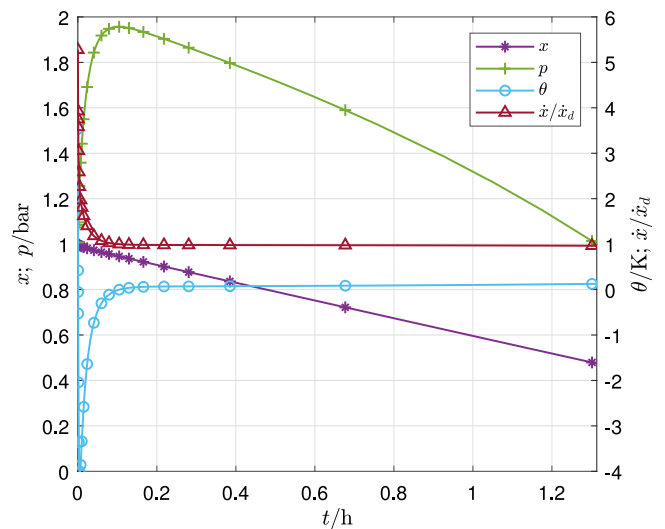

Fig. 5. Constant-flow rate discharge process of a NEC-based hydrogen storage system; theoretical discharge duration $\tau_{\max} = 2.5\,\text{h}$ (dimensionless power $\Pi = 23.6\,\%$, utilisation factor 52.5%).

the required theoretical discharge duration of 2.5 h clearly leads to a quite inefficient use of the storage system, as it can operate at constant power output only for just over 1.3 h, with a utilisation factor of 52.5%.

The Ragone plot obtained with the full model is represented, for LaNi$_5$- and NEC-based systems, in Fig. 6, and compared to the analytical results of the simplified model: the agreement between the two is remarkable, meaning that the performance is mainly determined by the kinetic equation, included in the simplified model, while the mass and energy conservation equations play a less decisive role. The only relevant divergence between the full and simplified model is observed for MH-based systems at high specific power output, close to the theoretical maximum: this is due to the mass of hydrogen that is available for discharge in the buffer, thanks to the initial pressure being higher than the minimum pressure. This mass can be released by the system under any operating conditions because it is already desorbed by the MH before the discharge process starts; however, there is a relatively small amount of hydrogen in the buffer, which explains why the two models diverge only at very high discharged flow rates.
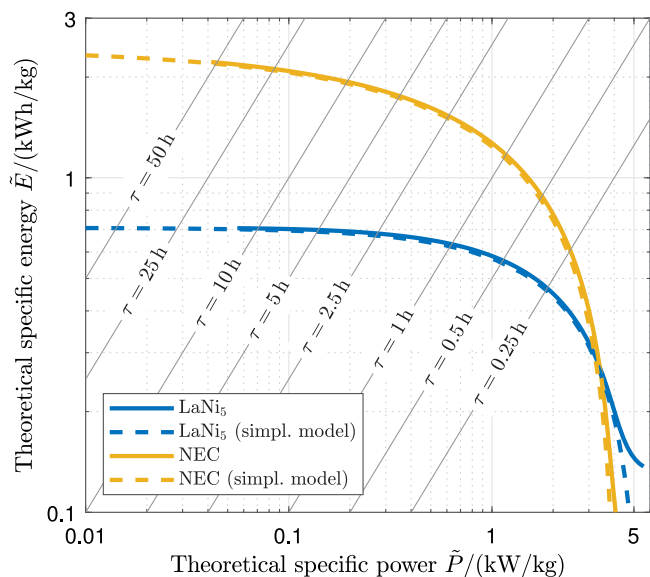
Fig. 6. Ragone plot of hydrogen storage systems based on LaNi$_5$ and NEC: comparison between the analytical results obtained with the simplified model and the numerical results of the full model.

Fig. 7. Ragone plot of hydrogen storage systems based on LaNi$_5$ and NEC: influence of hydrogen buffer volume. Continuous lines: base case; dotted lines: buffer volume halved with respect to the base case; dash–dot lines: buffer volume twice the base case.

Since the simplified and full model produce very similar results, the same general remarks are still valid for the full model: low-temperature MHs are characterised by lower specific energy values than LOHCs; however, at least for the materials considered in this example, MHs can be discharged more effectively (i.e. with a higher utilisation factor) over a wider range of specific power, mainly due to the first-order kinetic, providing utilisation factors up to approximately 80% for a discharge duration as low as 0.5 h.

The thermodynamic model parameters required by the governing equations, introduced in Section 2.4.1, have only marginal effects on the Ragone plot, as they mainly influence the system's initial transient thermal response, which lasts only for a fraction of the discharge duration (see Figs. 4 and 5), and therefore negligibly affect how long the system can sustain a constant-flow rate discharge process (clearly this is not the case for the kinetic model parameters, which instead have a significant impact on the Ragone plots, as discussed in Section 3.1). However, this is true if the heat transfer process is effective enough and the average temperature of the active mass is close enough to the required value: this could be challenging in the case of MH reactors, but several strategies to reach acceptable values of heat transfer effectiveness have been successfully modelled and tested, such as, for example, using phase-change materials and metal foams [36]. The only significant impact is related to the tail of the Ragone plots of MHs, which depends on the gaseous hydrogen available in the buffer, as proved by Fig. 7, which presents Ragone plots obtained with the full model for different values of the buffer available to gaseous hydrogen and hence for different values of the parameter ρ_{max}, which has been halved or doubled with respect to the base case. Very similar results, that is, almost indistinguishable Ragone plots, are obtained if the other model parameters are varied within reasonable ranges.

It must be observed that the full model here presented is also the result of a simplified analysis of reactor performance: in particular, it does not consider the actual layout of the model, the several equations needed to calculate the heat transfer effectiveness, or the real implementation of the control systems (the reactor pressure is here considered as the only control variable, while HTF temperature and flow rate could also be used [24]). As stated previously, it is nonetheless useful as a minimal working model that allows to capture the most relevant aspects of the discharge process in a simple yet effective way: even though the results obtained with more complete models would be
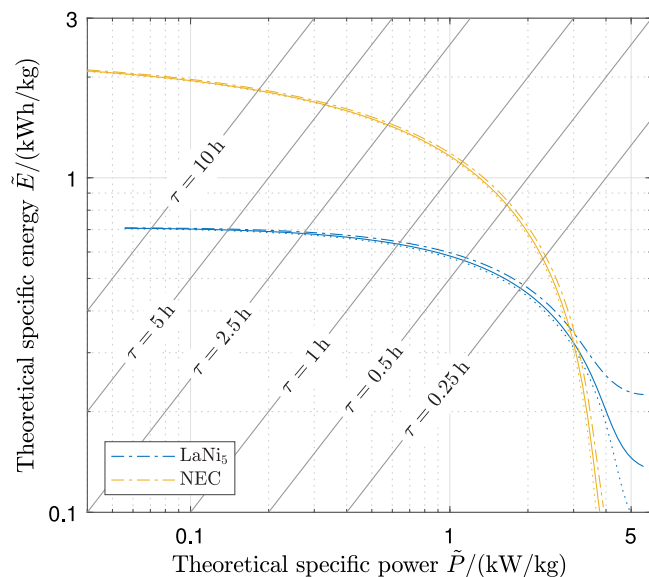
slightly different, the Ragone plots described here are still useful as they provide indications about the range of operating conditions that make these hydrogen storage systems work efficiently. These operating conditions depend mainly on the kinetics of the dehydrogenation/desorption reaction, which means that the same storage material can produce even significantly different results in terms of the energy–power relation if the reactor parameters that affect the kinetics (e.g., catalyst properties in the case of LOHCs, reactor layout) are changed. Moreover, practical implementation could lead to additional or more severe constraints on operating conditions: for example, the system is usually operated so that the degree of hydrogenation does not change over the full 0–1 range, so the maximum flow rate is lower than the value predicted by Eq. (33) because $x_0 < 1$; or the back pressure set by the end user results in a higher discharge pressure than $p_{min} = 1$ bar. A final caveat regarding the validity of the results presented in this paper is that the specific energy and power are obtained per unit of active substance mass, and this is why they were labelled as theoretical in Figs. 3, 6 and 7: as already noted previously, the total mass of the storage system is obviously higher than that of just the active mass, and as a consequence the Ragone plots of real material-based hydrogen storage systems are shifted down and to the left because of the lower values of specific energy and power.

4. Conclusions

Ragone plots are useful tools to describe the performance of energy storage systems in terms of energy that can be effectively delivered to an end user when it requires a constant power, and have been applied in different fields, such as electrochemical, mechanical, thermal storage systems. In this paper, Ragone plots of hydrogen storage systems have been introduced, with reference to material-based hydrogen storage such as MHs and LOHCs; the energy and power discharged by the storage system are matched to the hydrogen mass and mass flow rate, respectively, delivered to the end user and must be understood as the chemical energy (or power) carried by hydrogen.

Analytical expressions of the Ragone plots were first derived for these systems under the simplifying assumptions of a constant reactor temperature and a constant rate of dehydrogenation. In the case of LOHCs, the discharged dimensionless energy depends only on the

dimensionless power and the reaction order characterising the dehydrogenation kinetics; MHs exhibit a behaviour very close to the first-order kinetics, with a correction related to the slope of the desorption plateau. In terms of maximum specific energy, LOHCs are obviously favoured by the higher gravimetric density, resulting in a theoretical specific energy of 2–3 kWh/kg (chemical energy per unit mass of the active substance), while low-temperature MHs are limited to 0.4–0.8 kWh/kg. However, the second-order dehydrogenation kinetics of prominent LOHCs such as DBT and NEC means that the utilisation factor (the amount of hydrogen that can actually be delivered to the end user divided by the total amount of hydrogen stored) decreases much faster than MHs with an increase in specific power: acceptable values of the utilisation factor are feasible only if the discharge duration remains above a few hours, while it can be as low as 0.25 h in the case of $LaNi_5$.

Once the above-mentioned simplifying assumptions are removed, the numerical results obtained with the solution of the ODEs representing a minimal model of the storage system are very close to the analytical expressions resulting from the simplified model, proving that the system behaviour is mostly influenced by the reaction kinetics and that the simplified model can identify the efficient range of applications of a hydrogen storage system: LOHCs can sustain a specific power approximately in the range 0.05–1 kW/kg, with a discharge duration of around 2–25 h, depending on the kinetic performance of the particular LOHC considered; low-temperature MHs can work efficiently with slightly higher values of specific power, up to around 2 kW/kg, or a discharge duration of the order of 0.25 h.

Nomenclature

a	–	MH-related dimensionless coefficient
A	–	Coefficient for MH equilibrium pressure evaluation
b	1/Pa	Pressure coefficient
C	J/(kg K)	Heat capacity
$\dot{C}$	W/(kg K)	Flow heat capacity
ΔH	J/kg	Reaction enthalpy change
ΔS	J/(kg K)	Reaction entropy change
e	–	Dimensionless discharged energy
E	J	(Chemical) energy
E_a	J/(mol K)	Activation energy
k_0	1/s	Pre-exponential factor
K	–	Coefficient for MH equilibrium pressure evaluation
m	kg	Mass
M	kg/mol	Molar mass
$\dot{m}$	kg/s	Mass flow rate
n	–	Reaction order
p	Pa	Pressure
P	W	(Chemical) power
$\dot{Q}$	W	Heat rate
R	8.3145 J/(mol K)	Universal gas constant
t	s	Time
T	K	Temperature
U	J	Internal energy
V	m^3	Gaseous hydrogen volume
x	–	Degree of hydrogenation, hydrogen concentration
w	–	Gravimetric storage capacity

Greek letters

δ	K	Steady-state HTR-reactor temperature difference
ε	–	Heat transfer effectiveness
θ	K	Temperature-related system variable
Π	–	Dimensionless power
ρ	kg/m^3	Density
τ	s	Time constant, or discharge duration
ϕ	–	Coefficients for MH equilibrium pressure evaluation

Subscripts

0	Initial condition ($t = 0$)
d	Discharged
eq	Equilibrium
f	Related to HTF
hys	Hysteresis (related to MH equilibrium)
r	Reacted
sl	Plateau slope (related to MH equilibrium)
T	Thermal

Acronyms

DBT	DiBenzylToluene
DoH	Degree of Hydrogenation
HHV	Higher Heating Value
HTF	Heat Transfer Fluid
LOHC	Liquid Organic Hydrogen Carrier
MH	Metal Hydride
NEC	N-EthylCarbazole
ODE	Ordinary Differential Equation

References

[1] International Energy Agency, The future of hydrogen, 2019, URL https://www.iea.org/reports/the-future-of-hydrogen.

[2] World Energy Council, Hydrogen an enabler of the grand transition, 2018, URL https://www.worldenergy.org/assets/downloads/1Hydrogen-an-enabler-of-the-Grand-Transition_FEL_WEC_2018_Final.pdf.

[3] R. Gómez-Calvet, J.M. Martínez-Duart, A.R. Gómez-Calvet, The 2030 power sector transition in Spain: Too little storage for so many planned solar photovoltaics? Renew. Sustain. Energy Rev. 174 (2023) 113094, http://dx.doi.org/10.1016/j.rser.2022.113094.

[4] S. Bellocchi, P. Colbertaldo, M. Manno, B. Nastasi, Assessing the effectiveness of hydrogen pathways: A techno-economic optimisation within an integrated energy system, Energy 263 (2023) 126017, http://dx.doi.org/10.1016/j.energy.2022.126017.

[5] M. Robinius, A. Otto, P. Heuser, L. Welder, K. Syranidis, D.S. Ryberg, T. Grube, P. Markewitz, R. Peters, D. Stolten, Linking the power and transport sectors—Part 1: The principle of sector coupling, Energies 10 (7) (2017) 956, http://dx.doi.org/10.3390/en10070956.

[6] E. Zeyen, M. Victoria, T. Brown, Endogenous learning for green hydrogen in a sector-coupled energy model for Europe, Nature Commun. 14 (1) (2023) 3743, http://dx.doi.org/10.1038/s41467-023-39397-2.

[7] D. Tang, G.-L. Tan, G.-W. Li, J.-G. Liang, S.M. Ahmad, A. Bahadur, M. Humayun, H. Ullah, A. Khan, M. Bououdina, State-of-the-art hydrogen generation techniques and storage methods: A critical review, J. Energy Storage 64 (2023) 107196, http://dx.doi.org/10.1016/j.est.2023.107196.

[8] I.A. Hassan, H.S. Ramadan, M.A. Saleh, D. Hissel, Hydrogen storage technologies for stationary and mobile applications: Review, analysis and perspectives, Renew. Sustain. Energy Rev. 149 (2021) 111311, http://dx.doi.org/10.1016/j.rser.2021.111311.

[9] J. Andersson, S. Grönkvist, Large-scale storage of hydrogen, Int. J. Hydrogen Energy 44 (23) (2019) 11901–11919, http://dx.doi.org/10.1016/j.ijhydene.2019.03.063.

[10] B. Sakintuna, F. Lamari-Darkrim, M. Hirscher, Metal hydride materials for solid hydrogen storage: A review, Int. J. Hydrogen Energy 32 (9) (2007) 1121–1140, http://dx.doi.org/10.1016/j.ijhydene.2006.11.022.

[11] N. Klopčič, I. Grimmer, F. Winkler, M. Sartory, A. Trattner, A review on metal hydride materials for hydrogen storage, J. Energy Storage 72 (2023) 108456, http://dx.doi.org/10.1016/j.est.2023.108456.

[12] E. Díaz, P. Rapado-Gallego, S. Ordóñez, Systematic evaluation of physicochemical properties for the selection of alternative liquid organic hydrogen carriers, J. Energy Storage 59 (2023) 106511, http://dx.doi.org/10.1016/j.est.2022.106511.

[13] Y. Rong, S. Chen, C. Li, X. Chen, L. Xie, J. Chen, R. Long, Techno-economic analysis of hydrogen storage and transportation from hydrogen plant to terminal refueling station, Int. J. Hydrogen Energy (2023) http://dx.doi.org/10.1016/j.ijhydene.2023.01.187.

[14] G. Correa, F. Volpe, P. Marocco, P. Muñoz, T. Falagüerra, M. Santarelli, Evaluation of levelized cost of hydrogen produced by wind electrolysis: Argentine and Italian production scenarios, J. Energy Storage 52 (2022) 105014, http://dx.doi.org/10.1016/j.est.2022.105014.

[15] S. Jana, P. Muthukumar, Design, development and hydrogen storage performance testing of a tube bundle metal hydride reactor, J. Energy Storage 63 (2023) 106936, http://dx.doi.org/10.1016/j.est.2023.106936.

[16] P.T. Aakko-Saksa, C. Cook, J. Kiviaho, T. Repo, Liquid organic hydrogen carriers for transportation and storing of renewable energy – Review and discussion, J. Power Sources 396 (2018) 803–823, http://dx.doi.org/10.1016/j.jpowsour.2018.04.011.

[17] P. Krane, A.L. Nash, D. Ziviani, J.E. Braun, A.M. Marconnet, N. Jain, Dynamic modeling and control of a two-reactor metal hydride energy storage system, Appl. Energy 325 (2022) 119836, http://dx.doi.org/10.1016/j.apenergy.2022.119836.

[18] J.-H. Cho, S.-S. Yu, M.-Y. Kim, S.-G. Kang, Y.-D. Lee, K.-Y. Ahn, H.-J. Ji, Dynamic modeling and simulation of hydrogen supply capacity from a metal hydride tank, Int. J. Hydrogen Energy 38 (21) (2013) 8813–8828, http://dx.doi.org/10.1016/j.ijhydene.2013.02.142.

[19] D.O. Dunikov, V.I. Borzenko, D.V. Blinov, A.N. Kazakov, I.A. Romanov, A.I. Leontiev, Heat and mass transfer in a metal hydride reactor: combining experiments and mathematical modelling, J. Phys. Conf. Ser. 2057 (1) (2021) 012122, http://dx.doi.org/10.1088/1742-6596/2057/1/012122.

[20] J. Bollmann, N. Schmidt, D. Beck, P. Preuster, L. Zigan, P. Wasserscheid, S. Will, A path to a dynamic hydrogen storage system using a liquid organic hydrogen carrier (LOHC): Burner-based direct heating of the dehydrogenation unit, Int. J. Hydrogen Energy 48 (3) (2023) 1011–1023, http://dx.doi.org/10.1016/j.ijhydene.2022.09.234.

[21] A. Fikrt, R. Brehmer, V.-O. Milella, K. Müller, A. Bösmann, P. Preuster, N. Alt, E. Schlücker, P. Wasserscheid, W. Arlt, Dynamic power supply by hydrogen bound to a liquid organic hydrogen carrier, Appl. Energy 194 (2017) 1–8, http://dx.doi.org/10.1016/j.apenergy.2017.02.070.

[22] J. Geiling, M. Steinberger, F. Ortner, R. Seyfried, A. Nuß, F. Uhrig, C. Lange, R. Öchsner, P. Wasserscheid, M. März, P. Preuster, Combined dynamic operation of PEM fuel cell and continuous dehydrogenation of perhydro-dibenzyltoluene, Int. J. Hydrogen Energy 46 (72) (2021) 35662–35677, http://dx.doi.org/10.1016/j.ijhydene.2021.08.034.

[23] M. Gambini, F. Guarnaccia, M.L. Di Vona, M. Manno, M. Vellini, Liquid organic hydrogen carriers: Development of a thermodynamic and kinetic model for the assessment of hydrogenation and dehydrogenation processes, Int. J. Hydrogen Energy 47 (65) (2022) 28034–28045, http://dx.doi.org/10.1016/j.ijhydene.2022.06.120.

[24] M. Gambini, F. Guarnaccia, M. Manno, M. Vellini, Hydrogen flow rate control in a liquid organic hydrogen carrier batch reactor for hydrogen storage, Int. J. Hydrogen Energy (2023) http://dx.doi.org/10.1016/j.ijhydene.2023.05.153.

[25] D.V. Ragone, Review of Battery Systems for Electrically Powered Vehicles, SAE Technical Paper, 1968, 680453, http://dx.doi.org/10.4271/680453.

[26] T. Christen, M.W. Carlen, Theory of Ragone plots, J. Power Sources 91 (2) (2000) 210–216, http://dx.doi.org/10.1016/S0378-7753(00)00474-2.

[27] K. Yazawa, P.J. Shamberger, T.S. Fisher, Ragone relations for thermal energy storage technologies, Front. Mech. Eng. 5 (2019) 29, http://dx.doi.org/10.3389/fmech.2019.00029.

[28] T. Christen, Ragone plots and discharge efficiency-power relations of electric and thermal energy storage devices, J. Energy Storage 27 (2020) 101084, http://dx.doi.org/10.1016/j.est.2019.101084.

[29] M. Gambini, M. Manno, M. Vellini, Numerical analysis and performance assessment of metal hydride-based hydrogen storage systems, Int. J. Hydrogen Energy 33 (21) (2008) 6178–6187, http://dx.doi.org/10.1016/j.ijhydene.2008.08.006.

[30] J.E. House, Principles of Chemical Kinetics, Academic Press, 2007.

[31] D. Li, Y. Wang, L. Wu, F. Yang, Z. Wu, L. Zheng, J. Song, X. Zang, Z. Zhang, Kinetics study on the nonlinear modified varying-size model of LaNi$_5$ during hydrogenation/dehydrogenation, Chem. Eng. Sci. 214 (2020) 115439, http://dx.doi.org/10.1016/j.ces.2019.115439.

[32] F. Yang, Y. Zhang, F. Ciucci, Z. Wu, S. Wang, Y. Wang, Z. Zhang, Towards a consistent understanding of the metal hydride reaction kinetics: Measurement, modeling and data processing, J. Alloys Compd. 741 (2018) 610–621, http://dx.doi.org/10.1016/j.jallcom.2018.01.163.

[33] T.G. Voskuilen, E.L. Waters, T.L. Pourpoint, A comprehensive approach for alloy selection in metal hydride thermal systems, Int. J. Hydrogen Energy 39 (25) (2014) 13240–13254, http://dx.doi.org/10.1016/j.ijhydene.2014.06.119.

[34] L. Guo, Z. Wu, R. Li, X. Huang, B. Wang, F. Yang, Z. Zhang, New insights into the impurity transport and separation behaviours during metal hydride dehydrogenation for ultra-pure hydrogen, Appl. Energy 353 (2024) 122178, http://dx.doi.org/10.1016/j.apenergy.2023.122178.

[35] Y.T. Ge, P.Y. Lang, Performance analysis of a metal hydride refrigeration system, Appl. Therm. Eng. 234 (2023) 121264, http://dx.doi.org/10.1016/j.applthermaleng.2023.121264.

[36] A. Chibani, S. Merouani, C. Bougriou, The performance of hydrogen desorption from a metal hydride with heat supply by a phase change material incorporated in porous media (metal foam): Heat and mass transfer assessment, J. Energy Storage 51 (2022) 104449, http://dx.doi.org/10.1016/j.est.2022.104449.

[37] A. Züttel, Materials for hydrogen storage, Mater. Today 6 (9) (2003) 24–33, http://dx.doi.org/10.1016/S1369-7021(03)00922-2.

[38] M. Gambini, F. Guarnaccia, M. Manno, M. Vellini, Thermal design and heat transfer optimisation of a liquid organic hydrogen carrier batch reactor for hydrogen storage, Int. J. Hydrogen Energy 48 (96) (2023) 37625–37636, http://dx.doi.org/10.1016/j.ijhydene.2023.08.200.

[39] R. Peters, R. Deja, Q. Fang, V.N. Nguyen, P. Preuster, L. Blum, P. Wasserscheid, D. Stolten, A solid oxide fuel cell operating on liquid organic hydrogen carrier-based hydrogen – A kinetic model of the hydrogen release unit and system performance, Int. J. Hydrogen Energy 44 (26) (2019) 13794–13806, http://dx.doi.org/10.1016/j.ijhydene.2019.03.220.

[40] M. Witman, M. Allendorf, V. Stavila, Database for machine learning of hydrogen storage materials properties, 2022, http://dx.doi.org/10.5281/zenodo.7324809, [Data set]. Zenodo.

[41] R. Busqué, R. Torres, J. Grau, V. Roda, A. Husar, Mathematical modeling, numerical simulation and experimental comparison of the desorption process in a metal hydride hydrogen storage system, Int. J. Hydrogen Energy 43 (35) (2018) 16929–16940, http://dx.doi.org/10.1016/j.ijhydene.2017.12.172.